Ocean Dynamics (2004) 54: 250–265
DOI 10.1007/s10236-003-0073-4

Hans Burchard · Karsten Bolding · Manuel Ruiz Villarreal

Three-dimensional modelling of estuarine turbidity maxima in a tidal estuary

Received: 4 February 2003 / Accepted: 29 August 2003

Abstract A new numerical model for simulating estuarine dynamics is introduced here. This model, called General Estuarine Transport Model (GETM), has been specifically designed for reproducing baroclinic, bathymetry-guided flows where the tidal range may exceed the mean water depth in large parts of the domain such that drying and flooding processes are relevant. Several physical and numerical features of the model support exact and stable results for such domains. For the physics, high-order turbulence closure schemes guarantee proper reproduction of vertical exchange processes. Among the specific numerical features, generalised vertical coordinates, orthogonal curvilinear horizontal coordinates, high-order TVD advection schemes and stable drying and flooding algorithms have been implemented into GETM. The model is applied here to simulate the dynamics of estuarine turbidity maxima (ETMs), a complex feature present in most tidal estuaries. First, idealised simulations for a two-dimensional domain in the *xz* space will be shown to reproduce the basic generation mechanisms for ETMs. Then, a realistic three-dimensional simulation of the Elbe estuary in Northern Germany will be carried out. It is demonstrated that for a given forcing situation the model reproduces a stable ETM at the correct location.

Responsible Editor: Phil Dyke

H. Burchard (✉)
Baltic Sea Research Institute Warnemünde, Seestr. 15,
D-18119 Rostock-Warnemünde, Germany
e-mail: hans.burchard@io-warnemuende.de

K. Bolding
Bolding & Burchard Hydrodynamics GbR, Strandgyden 25,
DK-5466 Asperup, Denmark
e-mail: karsten@bolding-burchard.com

M. R. Villarreal
Manuel Ruiz Villarreal, Spanish Institute of Oceanography,
Muelle de Animas s/n, 15001 A Coruña, Galicia, Spain
e-mail: manuel.ruiz@co.ieo.es
(Formerly at Institute for Oceanography, University of Hamburg, Germany)

Keywords Numerical modelling · Turbulence · Stratified flow · Estuarine dynamics

1 Introduction

The aim of this paper is to present a numerical model for simulating estuarine dynamics. As a challenging test scenario, we selected the formation of estuarine turbidity maxima (ETMs) which depends sensitively on coupled current, stratification and turbulence interaction. These ETMs are zones of high-suspended matter concentrations which are trapped at certain locations in tidal estuaries. Several trapping mechanisms which act against the cross-sectionally averaged seaward transport have been identified in the literature. Here, we concentrate only on those which are related to longitudinal density gradients due to salinity penetrating into the estuary. Two major mechanisms for ETM formation near the landward tip of this salt intrusion are discussed in the literature. The residual gravitational circulation due to the longitudinal (along the main axis of the estuary) internal pressure gradient was first hypothesised by Postma and Kalle (1955) (see also Postma 1967). Festa and Hansen (1978) confirmed this hypothesis by means of a steady-state two-dimensional numerical model. Another process for the ETM formation was identified by Jay and Musiak (1994): internal tide asymmetry. In the presence of a longitudinal density gradient, sheared currents near the bed force a statically unstable stratification during flood and a statically stable stratification during ebb. This alternating process generates high vertical mixing rates during flood and low vertical mixing rates during ebb, which in turn result in near-bed velocity profiles which are more homogeneous during flood than during ebb. The tidal residual near-bed current is thus directed landwards. Both mechanisms prevent suspended matter (with its highest concentrations occurring near the bed) from being transported seawards. In a two-dimensional transient model study, Burchard and Baumert (1998) compared

the relevance of these two mechanisms for the formation of ETMs, with the result that the latter process (internal tide asymmetry) is more important than the former (residual gravitational circulation). This shows that ETMs are indeed the result of complex interaction between currents, stratification and turbulence and that their numerical simulation poses a challenging task.

Due to this physical complexity and the usually complicated estuarine bathymetry with extended intertidal flats, there is only a limited number of three-dimensional simulations for estuarine turbidity maxima. Lang et al. (1989) applied a finite-difference model to reproduce an extensive observational campaign in the lower Weser estuary in Northern Germany. They could explain most of the observations, but due to the limited simulation period (4.5 days), the formation process of the ETM itself could not be investigated. Similar conclusions were found by Malcherek (1995), who simulated the same campaign data by means of a three-dimensional finite element model. The same model had been successfully applied by Le Normant et al. (1998) to the Loire estuary in France, where the ETM is generated far upstream from the salt intrusion by means of barotropic mechanisms. Cancino and Neves (1999) could qualitatively reproduce suspended particulate matter (SPM) observations in the mesotidal Western Scheldt and in the macrotidal Gironde estuaries. Brenon and LeHir (1999) studied the importance of different processes in the generation of ETM in the Seine estuary. They report that in the macrotidal Seine, the barotropic distortion of the tidal wave (first studied in the Gironde by Allen et al. 1980) is the major effect, although also density effects influence the actual location of the ETM. For all these model simulations, the vertical turbulent exchange was parameterised by means of a simple algebraic mixing length approach. Transports calculated by means of a high-resolution finite-difference model (see Duwe 1988 and Duwe and Pfeiffer 1988) were used by Rolinski (1999) for driving a Lagrangian model for three size classes of suspended particulate matter in the Elbe estuary in Northern Germany. Although a simple, vertical mixing parameterisation with vertically constant eddy diffusivity was used, the formation of three distinct ETMs could be reproduced. For the Hudson River estuary in the northeast of the USA, a more complete simulation was carried out by Geyer et al. (1998), who applied the Blumberg and Mellor (1987) estuarine and coastal ocean model (ECOM). Similarly to the model presented here, a two-equation turbulence model, curvilinear horizontal coordinates and bottom and surface fitted coordinates were used. By means of their model simulation, Geyer et al. (1998) could successfully reproduce a turbidity maximum and its observed lateral variations.

Due to the important role of turbulent mixing for the formation of estuarine turbidity maxima (see Jay and Musiak 1994 and Burchard and Baumert 1998), the use of high-order turbulence models is a necessity for realistically simulating these features. Furthermore, some advanced numerical methods seem to be required in order to allow for using fairly coarse spatial resolutions without significantly loosing accuracy. Bottom-fitted coordinates allow for along-bed advection without steps (as in geopotential coordinate systems) introducing additional truncation errors. Surface-fitted coordinates allow for near-surface vertical discretisations which are finer than the tidal range. Curvilinear horizontal coordinates allow for horizontal meshes which are relatively fine in the cross-channel direction also for curved estuaries without the unnecessary and computationally expensive need of a fine longitudinal discretisation. The latter can also be achieved by means of finite elements which generally allow for higher flexibility in generating meshes due to the potentials of unstructured grids (see Le Normant et al. 1998). Furthermore, stable, non-diffusive and non-dispersive advection schemes are needed for accurately resolving fronts advected with the mean flow. Finally, stable and effective drying and flooding algorithms are needed for reproducing the dynamics of intertidal flats. Most of the models which combine these features are commercial products which are not freely accessible. The above-mentioned ECOM has just recently been made publicly available (A. Blumberg personal communication). The model MOHID is a semi-implicit model that incorporates drying and flooding and has been applied to simulation of estuarine dynamics (see Martins et al. 2001 and Villarreal et al. 2001), including ETM formation (Cancino and Neves 1999). So far however, it does not incorporate curvilinear coordinates. The recently developed regional ocean model system (ROMS, see Haidvogel et al. 2000, Ezer et al. 2002) has now been upgraded by including higher-order turbulence models (see Warner et al. 2003, Submitted, who used a two-dimensional channel with an ETM formation scenario as a test case). After the inclusion of a drying and flooding algorithm, also ROMS might be suitable for simulating tidal estuaries with realistic bathymetry.

This relatively low number of publicly available models for realistically simulating estuarine dynamics motivated us to develop a new model called GETM (General Estuarine Transport Model, see Burchard and Bolding 2002), which contains all the necessary features mentioned above. The ability of GETM to realistically simulate unstratified Wadden Sea dynamics has already been shown by Stanev et al. (2003). A comparative study between GETM and other three-dimensional models for an annual simulation of the North Sea is presented by Stips et al. (2003). It is the purpose of this paper to demonstrate the capability of GETM in reproducing estuarine dynamics and specifically its predictability for estuarine turbidity maxima. It is, however, not its purpose to provide a quantitative validation of GETM for estuarine flows with realistic forcing. Quantitative accuracy is usually dependent on the availability of validation data for periods for which accurate forcing data are at hand. The ETM in the Elbe estuary is a characteristic phenomenon, but it is subject to

spatiotemporal variability at different scales. Spatial variations in the location and shape of the ETM exist at tidal and subtidal time scales, as described in Kappenberg et al. (1995) and Rolinski (1999), and are also evident in the results we will present. Also, transient situations like freshwater avenues have a strong impact on the ETM, and can eventually wash it out of the estuary (Kappenberg et al. 1995). This high spatiotemporal variability, together with the difficulty of obtaining SPM data for long periods, the whole water column and at different points of the estuary, implied that quantitative model validation is difficult. Another complication is that, due to dredging activities and natural morphodynamics, realistic bathymetrical data, which are valid for a certain short period consistent with forcing and validation data, are not available.

The paper is structured as follows: in Section 2, the physical equations are discussed on which GETM is based; in Section 3 the numerical principles are given, especially the spatial discretisation (Sect. 3.1), the temporal discretisation (Sect. 3.2), the advection schemes (Sect. 3.3) and the drying and flooding algorithm (Sect. 3.4); in Section 4, the formation of estuarine turbidity maxima is simulated with Section 4.1 giving the suspended matter equations, Section 4.2 presenting results from idealised two-dimensional simulations and Section 4.3 presenting results from three-dimensional simulations of the tidal Elbe in Northern Germany. Finally, some conclusions are given in Section 5.

2 Model physics

For geophysical coastal sea and ocean dynamics, usually the three-dimensional hydrostatic equations of motion with the Boussinesq approximation and the eddy viscosity assumption are used (Bryan 1969; Cox 1984; Blumberg and Mellor 1987; Haidvogel and Beckmann 1999; Kantha and Clayson 2000). Since the formulation of the present model specifically considers coastal and estuarine domains where drying and flooding of mudflats plays a significant role, some simplifications of the model physics will be applied for very shallow water (of the order of less than 0.1 m). In such cases, it is not the proper description of the physics which is important but the stability of the model and the prevention of unphysical negative water depths (i.e. the production of virtual water). Thus, processes like rotation and advection will be neglected when the water becomes very shallow such that a simple balance between external pressure gradient and friction remains. With the non-dimensional damping factor α (see Eq. 6), which varies linearly between unity (deep water) and zero (very shallow water), the flux form of the dynamic equations of motion for the horizontal velocity components can be written in Cartesian coordinates as:

$$\begin{aligned}\partial_t u + \partial_z(uw) - \partial_z[(\nu_t+\nu)\partial_z u] + \alpha(\partial_x(u^2) + \partial_y(uv) \\ - \partial_x(2A_h^M\partial_x u) - \partial_y[A_h^M(\partial_y u + \partial_x v)] \\ - fv - \int_z^\zeta \partial_x b\,dz') = -g\partial_x\zeta \ , \end{aligned} \tag{1}$$

$$\begin{aligned}\partial_t v + \partial_z(vw) - \partial_z[(\nu_t+\nu)\partial_z v] + \alpha(\partial_x(vu) + \partial_y(v^2) \\ - \partial_y(2A_h^M\partial_y v) - \partial_x[A_h^M(\partial_y u + \partial_x v)] \\ + fu - \int_z^\zeta \partial_x b\,dz') = -g\partial_y\zeta \ . \end{aligned} \tag{2}$$

The vertical velocity equation reduces to the continuity equation:

$$\partial_x u + \partial_y v + \partial_z w = 0 \ . \tag{3}$$

Here, u, v and w are the ensemble averaged velocity components with respect to the x, y and z direction, respectively. The vertical coordinate z ranges from the bottom at $-H(x,y)$ to the surface at $\zeta(t,x,y)$ with t denoting time. ν_t is the vertical eddy viscosity, ν the kinematic viscosity, f the Coriolis parameter, and g is the gravitational acceleration. The horizontal mixing is parameterised by terms containing the horizontal eddy viscosity A_h^M, see Blumberg and Mellor 1987. The buoyancy b is defined as:

$$b = -g\frac{\rho-\rho_0}{\rho_0} \ , \tag{4}$$

with the density ρ and a reference density ρ_0. The last term on the left hand sides of Eqs. (1) and (2) are the internal (due to horizontal density gradients) and the terms on the right hand sides are the external (due to surface slopes) pressure gradients. In the latter, the deviation of surface density from reference density is neglected (see Burchard and Petersen 1997). The derivation of Eqs. (1)–(3) has been demonstrated in numerous publications, see e.g. Pedlosky (1987); Haidvogel and Beckmann (1999); Burchard (2002). In hydrostatic three-dimensional models, the vertical velocity is calculated by means of the continuity Eq. (3). Due to this, mass conservation and free surface elevation can easily be obtained.

Standard boundary conditions are applied for the horizontal momentum equations with a no-slip condition at the bed ($u = v = 0$ for $z = -H$) and a surface momentum flux applied at $z = \zeta$ calculated as a function of meteorological parameters such as wind speed. However, since wind stress plays a minor role in the formation of ETMs, the present calculations are carried out with zero surface forcing. In combination with kinematic boundary conditions, (near boundaries the flow is parallel to the boundary), a sea-surface elevation equation is derived by vertically integrating Eq. (3):

$$\partial_t\zeta = -\partial_x\int_{-H}^{\zeta} u\,dz - \partial_y\int_{-H}^{\zeta} v\,dz \ . \tag{5}$$

The non-dimensional factor α which equals unity in regions where a critical water depth D_{crit} is exceeded and approaches zero when the water depth D tends to a minimum value $D_{\min}$ is calculated as:

$$\alpha = \min\left\{1, \frac{D - D_{\min}}{D_{\text{crit}} - D_{\min}}\right\} \ . \tag{6}$$

Thus, $\alpha = 1$ for $D \geq D_{\text{crit}}$, such that the usual momentum equations result except for very shallow water, where simplified physics are considered with a balance between tendency, friction and external pressure gradient. In a typical wadden sea application, D_{crit} is of the order of 0.1 m and $D_{\min}$ of the order of 0.02 m (see Burchard 1998). Since for the steady-state between friction and pressure gradient, a velocity profile close to a logarithmic profile is obtained (see Nezu and Nakagawa 1993), the friction dominates in such a way that for water depths approaching zero the current velocities converge to zero as well. This has the effect that negative water depths are avoided due to Eq. (5). The numerical discretisation of the momentum Eqs. (1) and (2) requires some additional measures for avoiding negative water depths, see Section 3.4.

The conservation equations for tracers c^i with $1 \leq i \leq N_c$ (with N_c being the number of tracers), which can be e.g. temperature, salinity, nutrients, phytoplankton, zooplankton, suspended matter, chemical concentrations etc. is given as:

$$\partial_t c^i + \partial_x(uc^i) + \partial_y(vc^i) + \partial_z[(w + w_s^i)c^i] - \partial_z(\nu_t' \partial_z c^i) - \partial_x(A_h^T \partial_x c^i) - \partial_y(A_h^T \partial_y c^i) = Q^i \ . \tag{7}$$

Here, ν_t' denotes the vertical eddy diffusivity and A_h^T the horizontal diffusivity. Vertical migration of concentration with migration velocity w_s^i (positive for upward motion) is considered as well. This could be settling of suspended matter or active migration of phytoplankton. Q^i denotes all internal sources and sinks of the tracer c^i. This might, for example, be for the temperature equation the heating of water due to absorption of solar radiation in the water column.

The eddy viscosity ν_t (for momentum) and eddy diffusivity ν_t' (for tracers) need to be parameterised by means of turbulence models. Such models may range from simple algebraic prescription of profiles of ν_t and ν_t' (see Perels and Karelse 1982), via zero-, one, or two-equation models (see e.g. Luyten et al. 1996) to full Reynolds stress closure models (see e.g. Launder et al. 1975). In GETM, a compromise between accuracy and computational effort is made in such a way that usually two-equation models are used.

The most general form of a two-equation model has been recently suggested by Umlauf and Burchard 2003. The first equation is the standard dynamic equation for the turbulent kinetic energy (TKE), k:

$$\partial_t k - \partial_z\left[\left(\nu + \frac{\nu_t}{\sigma_k}\right)\partial_z k\right] = P + B - \varepsilon \ , \tag{8}$$

while the second equation is a non-linear combination of k and L with

$$L = \left(c_\mu^0\right)^3 \frac{k^{3/2}}{\varepsilon} \ , \tag{9}$$

denoting the macro (integral) length scale of the turbulence:

$$\partial_t(k^m L^n) - \partial_z\left[\left(\nu + \frac{\nu_t}{\sigma_{mn}}\right)\partial_z(k^m L^n)\right] = k^{m-1} L^n (c_{1mn} P + c_{3nm} B - c_{2nm}\varepsilon) \ . \tag{10}$$

On the right hand side of Eq. (8), ε denotes the dissipation rate of the TKE, and

$$P = \nu_t\left[(\partial_z u)^2 + (\partial_z v)^2\right], \quad B = -\nu_t' \partial_z b \ , \tag{11}$$

the shear and buoyancy production, respectively. Special cases of Eq. (10) are the k-ε model with $m = 3/2$ and $n = -1$ (see e.g. Burchard and Bolding 2001) or the k-ω model with $m = 1/2$ and $n = -1$ (see Wilcox 1998 and Umlauf et al. 2003). However, also the well-known Mellor and Yamada 1982 model with $m = 1$ and $n = 1$ fits into this concept after some modifications due to the necessary wall proximity function, see Umlauf and Burchard (2003).

From k and L, the eddy viscosity and diffusivity can finally be calculated by the following relations:

$$\nu_t = c_\mu k L, \quad \nu_t' = c_\mu' k L \ . \tag{12}$$

Here, c_μ and c_μ' are the stability functions, usually depending on shear, stratification and turbulent time scale, $\tau = k/\varepsilon$ (for an overview, see Burchard 2002).

Various sets of stability functions, which contain second-moment closure assumptions, have been suggested. The most successful in terms of comparison to laboratory and field data seems to be the closure introduced by Canuto et al. (2001). The dampening effect of stable stratification on turbulence is incorporated into these turbulence models by setting the steady-state Richardson number to $R_i^{st} = 0.25$ (for details, see Burchard and Bolding 2001). For all calculations of turbulence parameters, the turbulence module of the Public Domain model GOTM (general ocean turbulence model, available in the world wide web at `http://www.gotm.net`), developed by Burchard et al. (1999), has been integrated into GETM.

3 Discretisation

3.1 Spatial discretisation

The spatial discretisation in GETM is carried out in such a way that optimal spatial resolution is obtained for shallow, narrow and curved estuaries with high tidal ranges. For the vertical discretisation, there are basically two feasible approaches: fixed z coordinates or bathymetry and surface following general vertical coordinates. For the fixed z coordinates to allow the

near-surface resolution being higher than the tidal range, the concept of drying and flooding of vertical cells was developed by Casulli and Cheng (1992) (see also Pfeiffer 1987 and Burchard 1995). Major disadvantages of this approach are the poor reproduction of along-bed advection and turbulence production due to the step-like representation of sloping beds. The prototype of terrain and surface following coordinates (σ coordinates with vertical cell heights being a fixed fraction of the actual water depth) has been introduced into numerical models for natural waters by Freeman et al. (1972). The concept of general vertical coordinates (see Kasahara 1974 and Deleersnijder and Ruddick 1992) in which layers are arbitrarily distributed in the vertical has been applied to ocean modelling by various authors, see e.g. Beckers 1991; de Kok (1992); Gerdes (1993); Song and Haidvogel (1994); Burchard and Petersen (1997), Madec et al. (1998); Pietrzak et al. (2002). The major disadvantage of general vertical coordinates is the numerical truncation error occurring at locations where isopycnals with high vertical density gradients intersect with coordinate surfaces as is usually the case in stratified waters over sloping bathymetry. Here, the second-order accurate internal pressure gradient discretisation by Blumberg and Mellor (1987) has been applied. For a more advanced, recently developed discretisation with a reduced truncation error, see Shchepetkin and McWilliams (2003). Isopycnal coordinates, using isopycnals as coordinate interfaces, are in principle also a type of general vertical coordinates. Although they do not have this above-mentioned disadvantage, they are practically not applicable in estuaries due to the large range of densities involved and the extensive areas of well-mixed or unstably stratified waters. There is some hope that the concept of grids vertically adapting to the density structure of the flow as recently suggested by Burchard and Beckers (2004), would improve this drawback of general vertical coordinates. Since near-bed horizontal advection and turbulence production are major processes in tidal estuaries, the concept of terrain- and surface-following coordinates has been adopted for GETM. It should be noted that compared to z coordinates, no extra numerical effort is required for discretising a model with general vertical coordinates.

Horizontally, the discretisation is carried out on an Arakawa C grid along curvilinear orthogonal coordinates (see e.g. Haidvogel and Beckmann 1999). In contrast to Cartesian coordinates, the latter has the advantage that (given a fixed number of grid cells) flows in curved estuaries are spatially better resolved when aligning the coordinates parallel to the shoreline. Since this is not fully feasible for natural shorelines, some additional masking out of land points is generally necessary, see Section 4.3.

After the definition of vertical coordinate interfaces and the horizontal discretisation, the domain is decomposed into prisms with variable height. The dynamic equations introduced in Section 2 are then formally integrated over these prisms. With this finite-volume approach, conservation of mass and matter is guaranteed due to the Gaussian theorem which states for conservation equations in flux form that the changes inside the volumes are exactly caused by the fluxes normal to the surfaces surrounding the volume. Sources and sink terms do surely cause extra (non-conservative) changes.

3.2 Temporal discretisation

In hydrostatic models, there are basically two modes which need to be properly resolved in time: the fast barotropic mode and the baroclinic mode, which is usually slower for subcritical environmental flows. For explicit temporal discretisations, these two modes have thus to obey two different time-stepping criteria. According to Beckers and Deleersnijder (1993), the barotropic (vertically integrated) mode for non-rotational flow (rotation is considered as a secondary process for estuarine dynamics) may be formulated as:

$$\Delta t < \min_{ij}\left[\frac{1}{2}\left(\frac{1}{\Delta x_{ij}}+\frac{1}{\Delta y_{ij}}\right)\sqrt{2gD_{ij}}\right]^{-1}, \tag{13}$$

with Δx_{ij} and Δy_{ij} denoting the local horizontal dimensions of the grid cell.

In contrast to this, the time step of the internal mode is depending only on the Courant number for advection:

$$\Delta t < \min_{ij}\left\{\frac{\Delta x_{ij}}{u_{ij}^{\max}}, \frac{\Delta y_{ij}}{v_{ij}^{\max}}\right\}, \tag{14}$$

with the local maximum horizontal velocities $u_{ij}^{\max}$ and $v_{ij}^{\max}$. In order not to punish the whole model with a small time step resulting from the external system, two different approaches of mode splitting have been developed in the past.

The first approach, in which the external mode is calculated implicitly in time, has been proposed by Madala and Piacsek (1977). This method is numerically stable (if advection is absent) for unconditionally long time steps. The temporal approximation is of second-order if semi-implicit treatment is chosen. In such models, the external and internal mode are generally calculated with the same time steps (see e.g. Backhaus 1985).

Another approach is to use different time steps for the internal (macro times steps Δt) and the external mode (micro time steps Δt_m). One of the first free surface models which has adopted this method is the Princeton ocean model (POM), see Blumberg and Mellor 1987. This method has the disadvantage that interaction terms are needed for the external mode and that the consistency between internal and external mode is difficult to obtain. The advantage of this method is that the free surface elevation is temporally well resolved which is a major requirement for models including flooding and drying. That is the reason why this method is adopted here. A sketch of the time-stepping organisation in

GETM is shown in Fig. 1. The formulation of the interaction terms has been described in detail by Burchard and Bolding (2002).

In grid cells which are very shallow (order of centimetres) due to drying and flooding processes, the vertical Courant number due to the settling of SPM may become much larger than unity, occasionally. The directional splitting of advection (see Sect. 3.3) allows for such situations to treat the vertical advection differently: whenever Courant numbers C greater than unity are found during the vertical advection step in an individual grid cell, the vertical advection in this cell is divided into $\tilde{C}$ substeps with a time step of $\Delta t/\tilde{C}$ and frozen vertical velocity. Here, $\tilde{C}$ is the next integer greater than C, such that for all substeps the relevant Courant number remains smaller than unity.

3.3 Advective and turbulent transport

The simulation of conservative flows with propagating high gradients of matter as they typically occur in tidal estuaries poses a challenging numerical problem. Numerical schemes are required which guarantee conservation, monotonicity and high-order approximation. For GETM, we adopted the concept of total variation diminishing (TVD) schemes incorporated into ocean models with variable grids as suggested by Pietrzak (1998). This method is based on a directional-split approach, where the advection is alternately calculated in the x, the y and the z direction. Higher order in time approximations are obtained by means of Strang (1968) splitting which first calculates half an x, half a y step, then a full z step, followed by another half y and half x step. For guaranteeing conservation of mass, directional-split continuity equations need to be solved together with the advection equations, see Pietrzak (1998). In GETM, the TVD limiters of van Leer (1979) (MUSCL, second-order), Roe (1985) (Superbee, second order) and Hundsdorfer and Trompert (1994) (P2_PDM, third order) have been implemented. In GETM, these advection schemes are also implemented for the advection of momentum and turbulence. In order to do this consistently, discrete horizontal and vertical transports have to be locally interpolated to the boundary of the reference box relevant for the transported quantity. Application of higher-order advection schemes (in contrast to the first-order upstream advection scheme) to coastal dynamics does significantly increase the residual flow velocities (see Burchard and Bolding 2002).

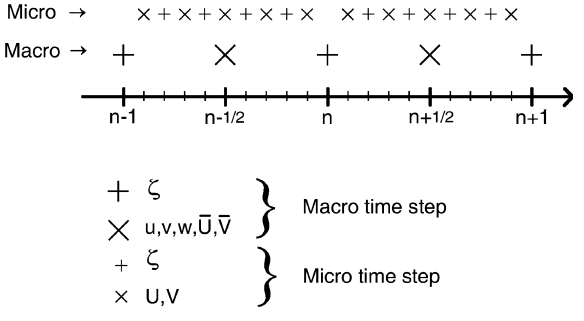

Fig. 1 Sketch explaining the organisation of the time stepping. Here, $\bar{U}$ and $\bar{V}$ are the vertically integrated transports averaged over one macro time step and U and V are the vertically integrated transports for each micro time step. The numbers n, $n+1/2$, ... denote numbers of full and intermediate macro time steps, respectively

3.4 Drying and flooding

Since usually large parts of tidal estuaries consist of intertidal flats, special care has to be taken to guarantee that the sea surface does not sink below the sea bed. In most estuarine or wadden sea models, this is incorporated by explicitly reducing the horizontal transports around a grid cell (see Flather and Heaps 1975). This, however, generally requires a complex set of rules how to reduce and increase these lateral transports into the grid cell. Furthermore, a noisy pattern of transports being switched on and off is generally observed (see Burchard 1995). We here follow a strategy which has already been suggested by Duwe 1988: to let the physics do most of the required flow reduction. Duwe (1988) and also Casulli and Cattani (1994) support this by calculating the depth of a transport point as the minimum of the depths of the two adjacent pressure points. This does, however, tend to underestimate the drainage of extensive intertidal flats during low water. In addition to the simplification of the momentum equations at very shallow water depths (factor α in Eqs. 1 and 2) GETM applies a correction to the barotropic pressure gradient in situations where the sea level in one grid cell is below the sea bed in an adjacent grid cell, for details see Fig. 2.

4 Modelling estuarine dynamics

The simulations presented in this section concentrate on modelling ETM formation, especially in the Elbe estuary, a mesotidal estuary in North Germany with extensive tidal flats.

4.1 Suspended sediment matter dynamics

Since this study focuses on the impact of hydrodynamics on sediment transport, a simple model for suspended particulate matter (SPM) with a single class of non-cohesive SPM particles that do not interact with the mean flow (no density effect of SPM) is considered. The concentration c of SPM is modelled with the tracer equation (see also Eq. 7):

$$\partial_t c + \partial_x(uc) + \partial_y(vc) + \partial_z[(w - w_s)c] - \partial_z(\nu'_t \partial_z c) - \partial_x\left(A_h^T \partial_x c\right) - \partial_y\left(A_h^T \partial_y c\right) = 0 \ , \qquad (15)$$

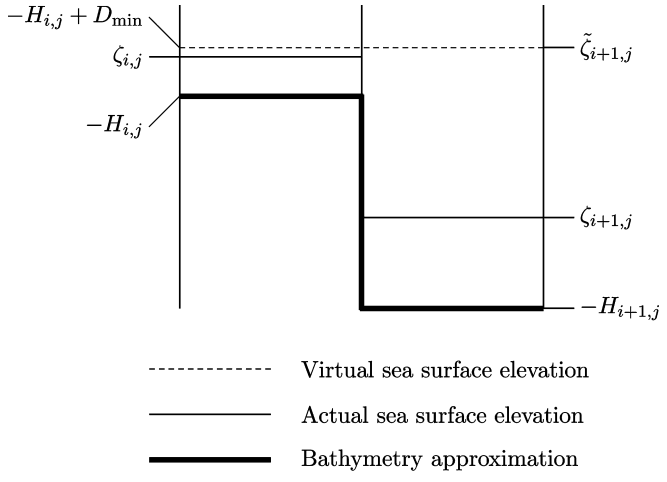

Fig. 2 Sketch explaining the principle of pressure gradient minimisation during drying and flooding over sloping bathymetry. The uncorrected pressure gradient would here be established by the difference between $\zeta_{i+1,j}$ and $\zeta_{i,j}$. Since $\zeta_{i+1,j}$ is lower than the adjacent sea bed at $z = -H_{i,j}$, the resulting pressure gradient is unphysically high and too much water would be transported out of the left grid cell. In order reduce this pressure gradient, the pressure gradient is calculated by means of the corrected difference between $\tilde{\zeta}_{i+1,j} = -H_{i,j} + D_{\min}$ and $\zeta_{i,j}$. In the case shown here, where already too much water has left the left grid cell, water is even flowing back. Due to the fact that the situation shown in this figure is vanishing with further grid refinement, the correction presented here is numerically justified

where w_s is the settling velocity of SPM, that will be set to a constant value of $w_s = 0.001\,\mathrm{m\,s^{-1}}$, which is characteristic for fine sediments in the Elbe estuary. At the open boundary, no flux conditions are imposed:

$$\partial_x c = 0 \ . \tag{16}$$

Also no flux of SPM through the surface is assumed:

$$w_s c + \partial_z (\nu_t' \partial_z c) = 0 \ . \tag{17}$$

At the bottom, the net SPM flux is the residual of erosion and sedimentation fluxes:

$$-w_s c - \partial_z (\nu_t' \partial_z c) = F_e - F_s \ , \tag{18}$$

where erosion and sedimentation fluxes are modelled following Krone (1962) as functions of the bottom shear stress τ_b. This parameterisation has been widely applied because of its simplicity and because it requires only few empirical parameters. The erosion flux is only non-zero when the bottom shear stress exceeds a critical shear stress τ_{ce}:

$$F_e = \begin{cases} \frac{c_e}{\rho_0}(|\tau_b| - \tau_{ce}), & \text{for } B > 0 \text{ and } |\tau_b| > \tau_{ce}, \\ 0, & \text{else} \ , \end{cases} \tag{19}$$

with $c_e = 0.5\,\mathrm{kg\,s^{-1}\,m^{-4}}$ and the fluff layer SPM content B (see below). The sedimentation flux is non-zero only for bottom shear stresses smaller than a critical shear stress τ_{cs}. This flux is limited by the near-bottom concentration c_b:

$$F_s = \frac{w_s c_b}{\tau_{cs}}(\tau_{cs} - |\tau_b|). \tag{20}$$

The selected values of critical shear stresses are based on empirical estimations in the Elbe estuary. The critical shear stress for erosion is set to $\tau_{ce} = 0.13\,\mathrm{N\,m^{-2}}$, and for sedimentation to a slightly lower value of $\tau_{cs} = 0.1\,\mathrm{N\,m^{-2}}$ (see Lobmeyr and Puls 1991). A pool B of non-dynamic particulate matter (fluff layer) is assumed in order to take into account the effects of depletion of erodible material at the bottom. A horizontally homogeneous distribution with $B = B_0 = 0.3\,\mathrm{kg\,m^{-2}}$ is initially assumed. Sedimentation and erosion fill and empty this pool, respectively:

$$\partial_t B = F_s - F_e \ , \tag{21}$$

and the erosion flux is constricted by the availability of SPM from the pool (see Eq. 19). The erosion and sedimentation fluxes are discretised using the quasi-implicit Patankar (1980) approach, which guarantees positivity of SPM.

4.2 Idealised flow simulation

This idealised model setup is based on the study by Burchard and Baumert (1998) with a two-dimensional domain. Dimensions and other relevant parameters (such as river runoff and suspended matter properties) are set to those characteristic for the Elbe estuary. A two-dimensional channel of $L = 100\,\mathrm{km}$ length and a constant depth of $H = 15\,\mathrm{m}$ is closed at the eastern boundary, where a weir in the real Elbe estuary exists. This constant water depth reflects the navigational channel which has been dredged all the way up to Hamburg harbour. Tidal forcing at the open boundary is an M_2 tide with an amplitude of 1.3 m. At the river boundary, a river runoff of $700\,\mathrm{m^3 s^{-1}}$, the most frequent value close to the long-term average value for the Elbe river (Kappenberg et al. 1995), is imposed. To represent the broadening of the estuary and the influence of well-mixed seawater at the open sea boundary, salinity is relaxed towards a value of 30 during the first 20 km, with a relaxation factor increasing towards the open sea. Temperature variations are neglected here. The horizontal spatial step is set to $\Delta x = 200\,\mathrm{m}$, and 30 equidistant σ layers in the vertical are considered, which results in a mean vertical step of $\Delta z = 0.5\,\mathrm{m}$. More sophisticated vertical coordinates were not necessary in this flat bottom numerical experiment. The micro time step is $\Delta t_m = 10\,\mathrm{s}$ and with $M = 5$, the macro time step is $\Delta t = 50\,\mathrm{s}$. The k-ε model with stability functions by Canuto et al. (2001) is used as turbulence model for the reference experiment. At the surface and the bottom, Neumann flux boundary conditions for k and ε are chosen (see Burchard and Petersen 1999).

The model has been run without computing SPM for 20 tidal cycles, when a periodic steady state is reached. The duration of this spin-up period until a steady state is approached depends mainly on the initial conditions for salinity. Afterwards, the whole model including SPM dynamics is reinitialised from this state with zero SPM

concentration in the water column and a horizontally homogeneous bottom pool B and run for further 20 tidal periods, when a clear quasi-periodic steady state in SPM is found.

In Figs. 3, 4 and 5 SPM concentration, velocity and eddy diffusivity overlaid on salinity contours for the first 50 km of the domain are shown for the periodic steady state. SPM concentration and eddy diffusivity are

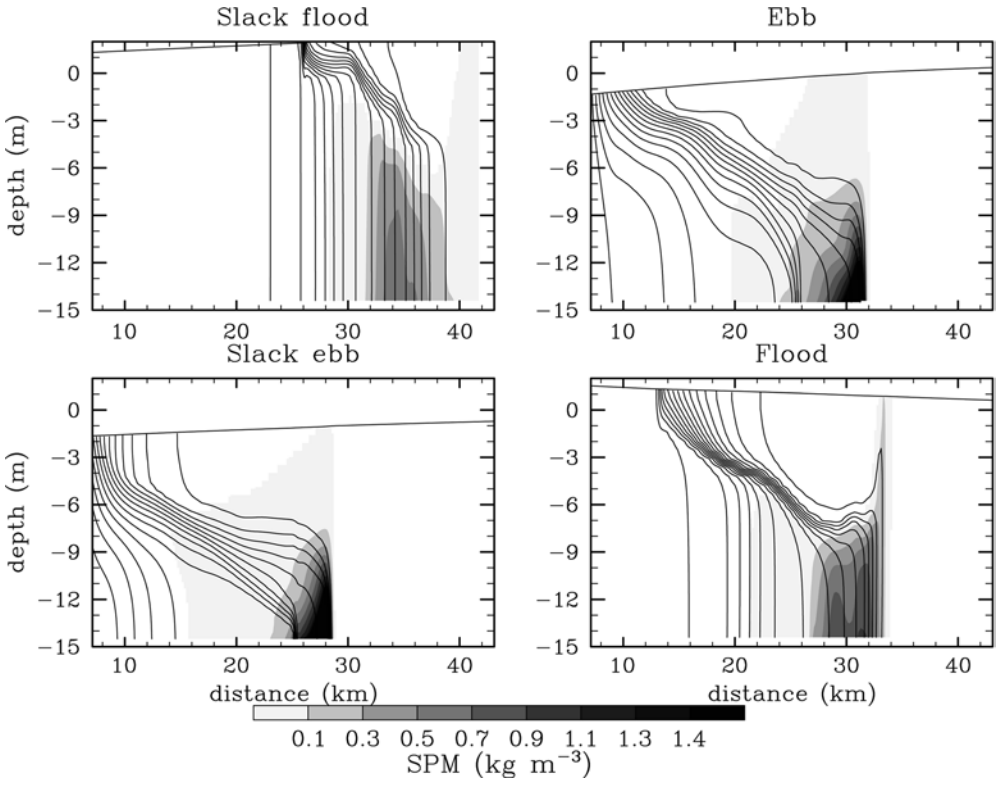

Fig. 3 SPM concentration (*shaded*) and salinity (contours from 2 to 30 psu with intervals of 2 psu) on the first 50 km of the two-dimensional domain for four tidal instants. A k-ε turbulence model and a Superbee advection scheme for momentum and tracers have been used

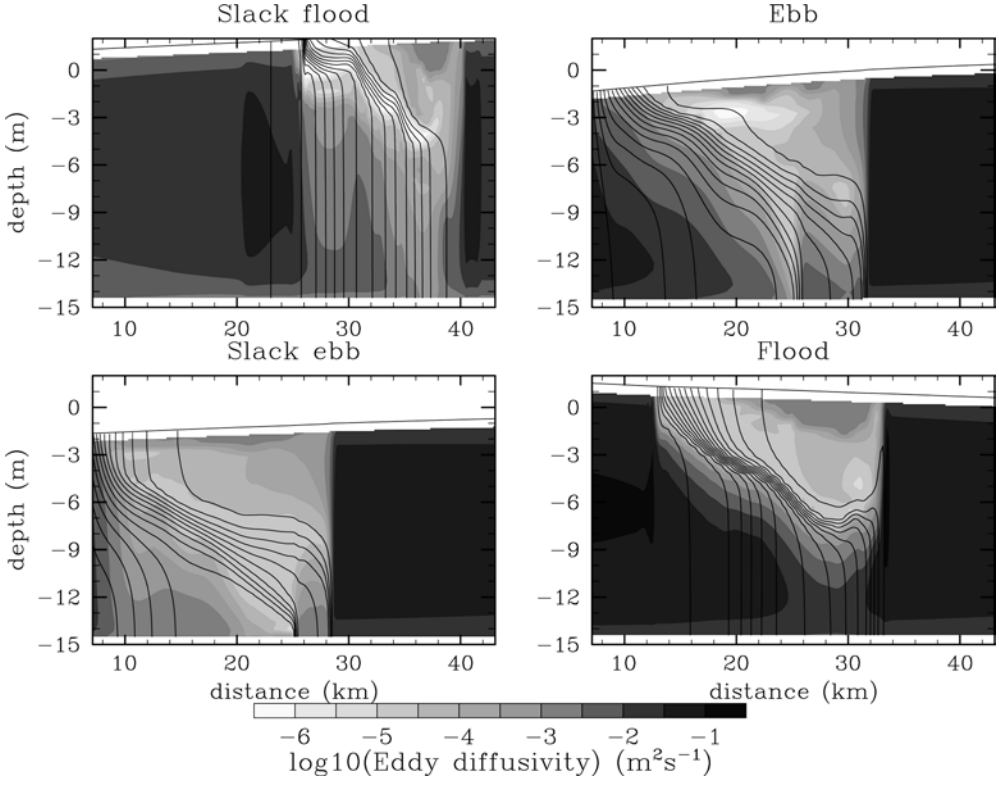

Fig. 4 Logarithm of eddy diffusivity (*shaded*) and salinity (contours from 2 to 30 psu with intervals of 2 psu) on the first 50 km of the two-dimensional domain for four tidal instants. A k-ε turbulence model and a Superbee advection scheme for momentum and tracers have been used

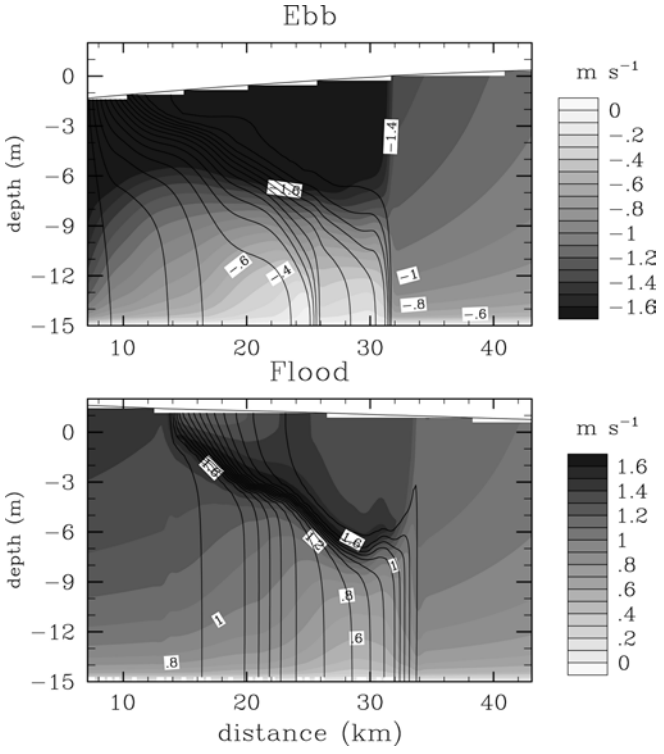

Fig. 5 Velocity in m s^{-1} (*shaded*) and salinity (contours from 2 to 30 psu with intervals of 2 psu) on the first 50 km of the two-dimensional domain for ebb and flood

plotted for four tidal instants: full tides (ebb and flood), which we define as the instant of maximum velocities, and slack tides (slack flood and slack ebb), when elevation reaches maxima or minima. Velocity is plotted only at full tides. The inspection of these figures provides us with a description of the basic physical phenomena in this idealised tidally strained density fluid.

During flood, denser salty water enters the estuary where fresher water exists, and advances faster, relative to symmetric tide, at the bottom. This process is opposite during ebb, when freshwater encounters the salty water and advances faster at surface layers. Bottom shear stresses are largest at full tides and have a minimum at slack tides. A salt wedge that moves back and forth with the tide is generated. The tip of this salt wedge penetrates around 40 km from the open boundary at slack flood. Also an ETM is generated near the tip of the salt wedge and develops within a few tidal periods.

During flood (Fig. 3d), the increase of bottom shear stress until full flood resuspends material that is advected with the ingoing current causing the maximum of SPM concentration near the tip of the salt wedge. The pycnocline gets thinner during the advance of the salt wedge. In the core of the pycnocline, the velocity shows a peak (Fig. 5b). After full flood (Fig. 3a), tidal velocities reduce and, correspondingly, bottom shear stresses, that reach a minimum at high water. The lower bottom shear stresses reduce the erosion rate and, at the end of the flood, also deposition takes place, leading to a reduction of the SPM concentration inside the ETM. During ebb (Fig. 3b), the current reverses and the bottom shear stress begins to increase, such that erosion takes place again. The reduction of velocities decreases erosion from full ebb on and sedimentation refills the bottom pool, that will then be resuspended during the next flood. The ETM is still present at low water (Fig. 3c), mainly because of the small settling velocities considered here.

This situation is further described in Fig. 4, where the logarithm of eddy diffusivity is represented for the same four tidal instants. Since no wind stress is considered, eddy diffusivities are low above the pycnocline. During flood, high values of near-bed eddy diffusivities are observed. The current shear causes the advance of saline water to be slower near the bottom such that an unstable salinity stratification is generated. This process enhances mixing below the pycnocline and pushes the pycnocline towards the surface. The low levels of turbulence at the pynocline contribute to the maintenance of the sharp maximum of velocity at the pycnocline, as put forward in Geyer and Farmer (1989). During ebb, the increase of shear erodes the pycnocline, and the stable stratification results in lower vertical diffusivities. This variation of mixing and stratification has an impact on velocity profiles. During flood (Fig. 5b), velocities are vertically more uniform and bottom-intensified, with respect to a symmetric tide. During ebb, currents are more intense at the surface (Fig. 5a). This velocity asymmetry resulting from the tidal straining of a density field was named internal tide asymmetry by Jay and Musiak (1994) (see Sect. 1). The basic processes represented by our model are very similar to those presented by Geyer and Farmer (1989) in the analysis of detailed measurements of tidal variations of velocity and salinity in the Fraser River, which described the asymmetries in stratification and velocities between ebb and flood.

We can conclude that the model is able to represent the main features of the physical process of strain-induced periodic stratification (SIPS, see Simpson et al. 1990), resulting from the interaction between tides and horizontal density gradients in regions of freshwater influence. In a comparison of dissipation rate measurements with model results with the one-dimensional water column model GOTM, Simpson et al. (2002) could show that second-order turbulence closures like those used in GOTM were suitable for reproducing the dissipation rate measurements, and consequently the basic features of SIPS. Our simulations in this setup reproduce not only the SIPS, but also the fact that the periodical variation of stratification generates an asymmetry between flood and ebb velocities (internal tide asymmetry Jay and Musiak 1994), that results in the appearance of an ETM. Although we have described the model results only in general terms (further details will be given in a forthcoming paper), the results show the ability of the present model to describe the interaction between stratification and tides involved in circulation and transport of sediments in partially mixed and strongly mixed estuaries.

4.3 Tidal Elbe simulation

The Elbe estuary (Fig. 6) comprises the lower 150 km of the Elbe River: from the weir at Geesthacht (not shown in Fig. 6) to the river mouth to the North Sea. The location of Hamburg harbour, one of the biggest harbours in Europe, about 100 km upstream of the river mouth implies intensive traffic of container ships. A great dredging effort is devoted to keep the river navigable. At the outer zone, the estuary gets broader and an extensive zone of tidal flats exists. The mean tidal range is of about 3 m, with flood shorter than ebb. A zone of increased sediment concentration is found near the limit of the salt intrusion (usually near Brunsbüttel) and extends over 30 km (see Kappenberg et al. 1995). Apart from this main ETM, there is evidence of secondary ETMs in the freshwater region (see Kappenberg et al. 1995 and Rolinski 1999).

We have constructed an orthogonal curvilinear grid of the Elbe estuary, that follows the shoreline (see Fig. 7). The freeware tool SeaGrid Orthogonal Grid Maker For Matlab (see http://woodshole.er.usgs.gov/staffpages/cdenham/public_html/seagrid/seagrid.html) was used for generating the grid and checking its orthogonality. The grid has 175×20 grid elements, which gives a mean longitudinal (along-channel) resolution of 500 m, with a varying across-channel resolution typically of less than 100 m. Due to the irregularity of the coastline, a masking of land points after constructing the grid was done. Depths at the grid points are computed by interpolation and smoothing of bathymetric data in a $25\,\mathrm{m} \times 25\,\mathrm{m}$ grid provided by the Bundesanstalt für Wasserbau Dienststelle Hamburg (BAW-AK).

The open boundary in our model is located at Cuxhaven. There, the tide is imposed by elevations based on a tidal harmonics analysis of the measured tide at Cuxhaven harbour. Only two tidal constituents there (M_2, M_4) are used in the forcing, representing the observed semidiurnal tide with a dominance of flood, but without spring–neap variations. Salinity at the open boundary is advected during outflow and relaxed to a characteristic value of 23 psu. Suspended sediment matter is advected during outflowing and no SPM is introduced during inflow (i.e. SPM is relaxed to zero).

In the simulations, we have used a micro time step of $\Delta t \approx 3.7$ s and a macro time step ten times longer. For the vertical discretisation, 20 equidistant σ layers have been used. Due to the complexity of the flow, we could not find any improvement by using more sophisticated vertical grid structures. A high-order advection scheme with the Superbee limiter has been used for advection of momentum, salinity and SPM concentration, see Section 3.3. The k-ε model with stability functions by Canuto et al. (2001) is used as the turbulence model. The parameters in the SPM model are the same as those chosen in Section 4.1.

We have applied a river runoff of $700\,\mathrm{m^3\,s^{-1}}$ at the eastern boundary. The model is run without SPM until a periodic quasi-stationary state in salinity is obtained. Afterwards, the SPM dynamics is initialised with a horizontally homogeneous pool of bottom SPM, except

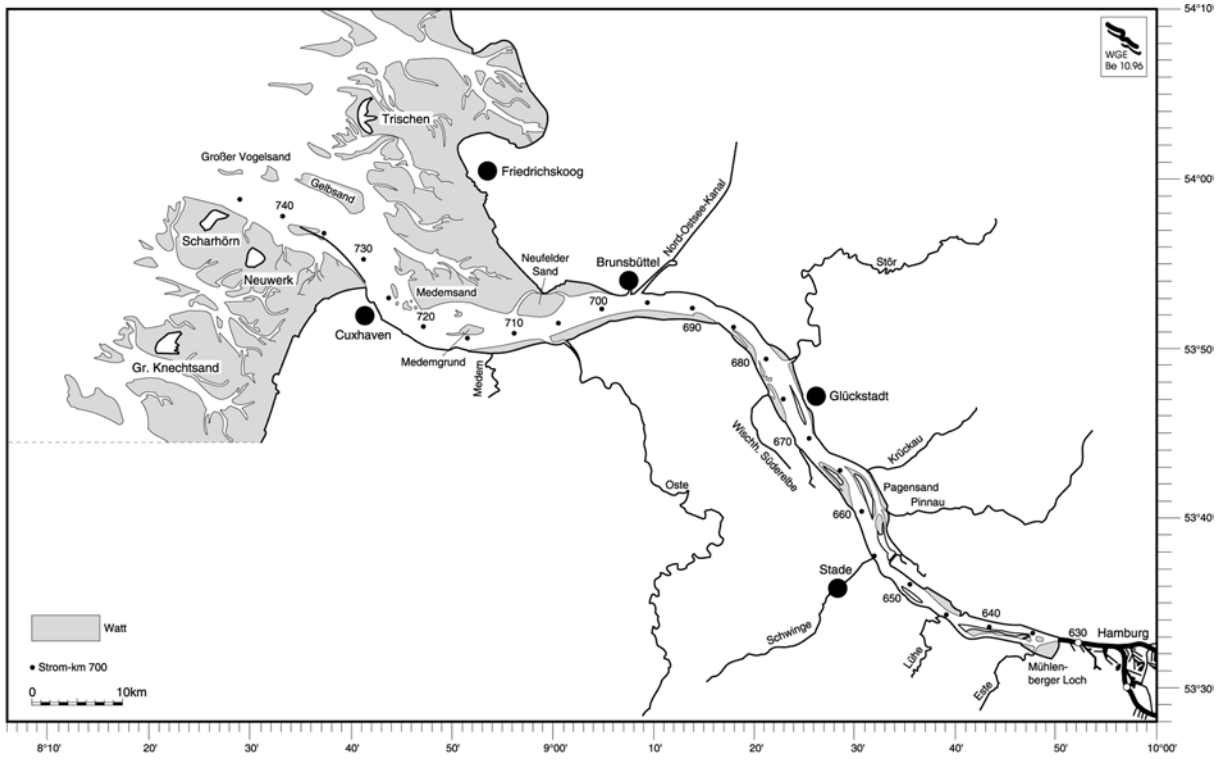

Fig. 6 Map of the lower Elbe estuary

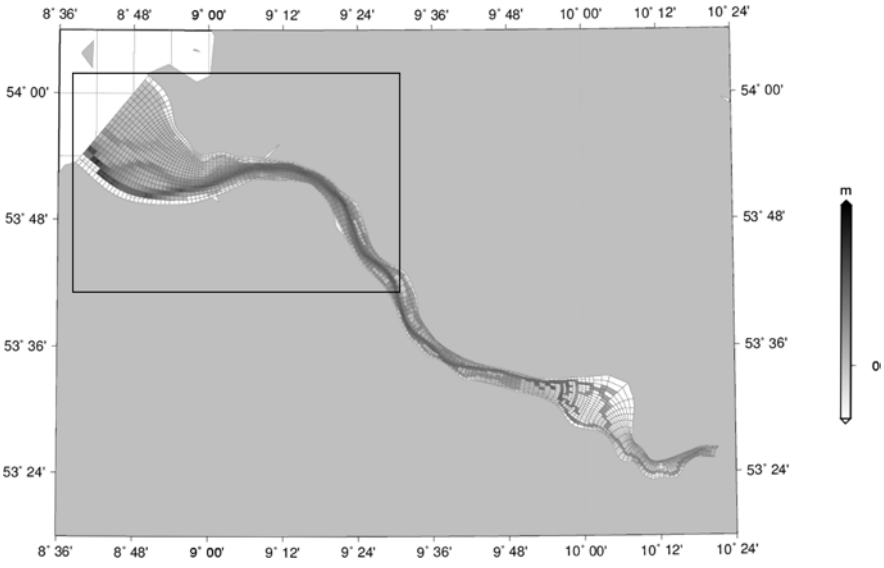

Fig. 7 Curvilinear grid and bathymetry used in the simulations. *Grey-shaded* polygons indicate the local depth inside the model domain, *white polygons* denote cells which have been considered as land points and were thus masked out. The *black rectangle* indicates the subdomain for which velocities and salinity and SPM concentrations are shown in Figs. 8 and 9

for the intertidal flats. No new erosion of wadden areas is therefore considered in our simulations, the only SPM in these areas is that previously advected. This simplification is motivated by the fact that erosion processes in intertidal flats are difficult to parameterise due to the specific phenomena there, that include consolidation in the drying phase and effects of vegetation and other organisms on erodibility. An initial homogeneous pool of SPM also in intertidal flats implies only more SPM in the domain and also more accumulation in the intertidal flats, especially to the north of the Medemsand area, but does not introduce more realism in our simulations. There is no external input of SPM in the model, and therefore no stationary distribution is found (the system is losing SPM), but after about 20 tidal cycles a quasi-stationary state in SPM is found, and the results will be shown for that period.

In Figs. 8 and 9, near bottom SPM concentration and velocity are plotted against salinity contours for four tidal phases: slack ebb and flood and full ebb and flood at km 690, between Brunsbüttel and the Stör mouth, where the mean location of the ETM appears. We can see how the model simulates the drying and flooding of intertidal zones. The light grey shaded zones correspond to points that have fallen dry. In the extense wadden area near the mouth: Medemsand, where intertidal zones and flooding channels are evident, the model stably computes velocity, salinity and SPM distribution. Velocities are stronger during flood in the main channel and reach values of more than $1.5\,\mathrm{m\,s^{-1}}$, similarly to the values reported by Kappenberg et al. (1995) and Rolinski (1999). A salinity intrusion (indicated by the 1 psu isohaline) progresses upstream during flood and reaches the Stör mouth. This salinity intrusion evolves with tide, similar to what is observed in the estuary for moderate or low runoff (see Kappenberg et al. 1995) and to the model results reported in Rolinski (1999). A maximum of SPM concentration upstream of the 1 psu salinity isohaline is found, that extends for some kilometres. This ETM is located at the southern part of the main navigational channel. The shape of the ETM varies with tidal phase, being more elongated during flood, when near-bottom velocities are larger than during ebb. The sequence of tidal SPM evolution can be described by inspecting Fig. 8. During flood, the deposited SPM pool is resuspended and advected upstream. At the end of flood, deposition takes place and therefore high near-bottom SPM concentrations are observed. The high SPM concentration to the north of the wadden area corresponds to SPM advected from the wadden areas that accumulates there. During ebb, the flood-deposited SPM and the SPM still in the water column are advected downstream and deposit again at slack ebb, when the maximum near-bottom SPM concentrations appear in our figures (see Fig. 8d). Also during ebb, a local maximum of SPM develops near Medemsand in the channel adjacent to the wadden area. This maximum probably results from the resuspension of SPM deposited in intertidal flats during flood that has being advected to this area during drying and deposited there. In this area a frontal structure results during ebb from the advection of saltier water in the wadden area (see Fig. 9) that encounters the fresher water advected from upstream during ebb (see Fig. 9). This frontal phenomenon has been previously described by Duwe (1988).

For the idealised forcing (simplified tide, runoff, no wind) which we have considered, a stable ETM appears near the limit of the salt intrusion, that extends for 30 km. The zone of SPM accumulation in our results corresponds with the location of the main ETM for average run-off (see Kappenberg et al. 1995). The ETM is generated from a uniform source of SPM at the bottom, and there is no need of tuning the initial distribution of SPM sources as has been done in the model simulations by Lang et al. (1989) in the Weser or

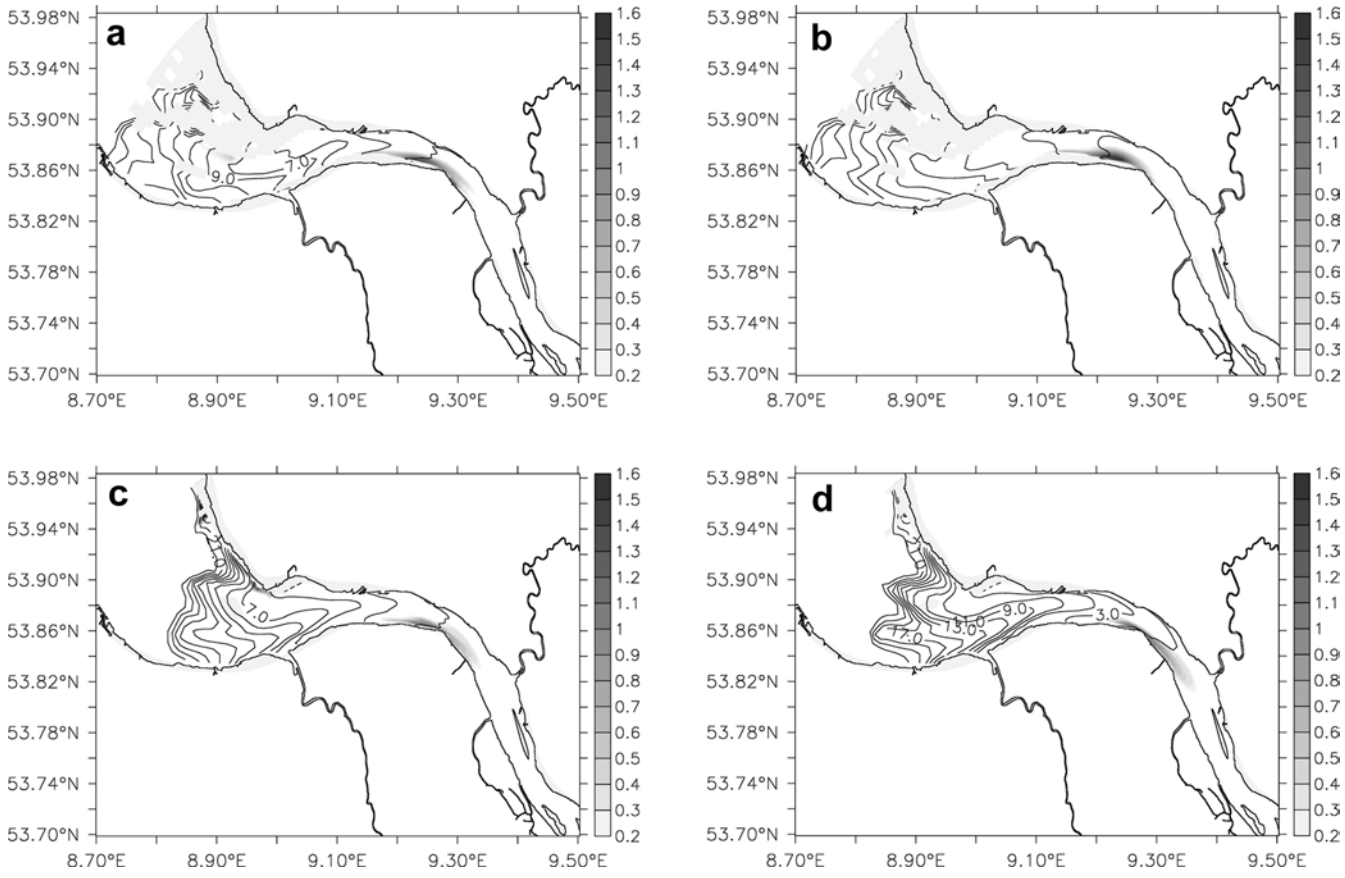

Fig. 8 Salinity (contours from 1 to 23 psu with intervals of 2 psu) and SPM concentration in kg m^{-3} (*shaded*) for flood tide (*upper left*), slack flood tide (*upper right*), ebb tide (*lower left*) and slack ebb tide (*lower right*) at km 690. *Light grey shaded areas* correspond to cells that have fallen dry

by Brenon and LeHir (1999) in the Seine, although the latter reports similar results for different initial SPM patterns. Therefore, the basic mechanism described in the idealised domain (Sect. 4.2) apparently is acting in the realistic domain and contributes to the trapping of SPM and generation of an ETM from the initial uniform source of SPM. The impact of across-channel circulation and curvature of the bathymetry on the ETM shape has not been studied, but the results put forward that these effects should be properly investigated to understand the ETM evolution in the estuary. It is not the purpose of the present study to give a detailed account of the performance of the model in simulating the hydrodynamics of the Elbe estuary. However, we must note that, with the forcing conditions in this model grid, we cannot reproduce all the details of the tidal wave propagation in the Elbe estuary. One of the reasons is that we consider a constant in space tidal forcing along the western open boundary, although the tidal signal at Cuxhaven (south side of the estuary) has a delay with respect to the north shore, especially during ebb, due to recirculation in the wadden area not fully covered in our simulation domain (see Dippner 1984 and Duwe 1988). However, the phase and amplitude of the tidal wave at different points of the estuary are reasonably well represented in our simulations. Another important feature is the fact that the tidal range in the Elbe estuary decreases from the inlet (around 3 m) towards Brunsbüttel (around 2.5 m), then increases to attain a maximum at Hamburg (3.5 m at Sankt Pauli) and falls to 2 m at the weir (see for example Kappenberg et al. 1995 and Rolinski 1999). Our model represents this phenomenon, but the amplification at Hamburg harbour is underestimated. Therefore, we are missing some effect of the barotropic tidal wave deformation that could be relevant for understanding SPM distribution in the Elbe, especially for understanding the ETM described in the freshwater region (see Kappenberg et al. 1995 and Rolinski 1999). We attribute this inconsistency to the still relatively coarse model resolution along the estuary, especially in the Hamburg harbour area and upstream. However, our simulations qualitatively reproduce the salinity intrusion and a stable ETM for these simplified forcing conditions. This is the first time that tide, density, turbulence and SPM have successfully been coupled in a three-dimensional model for the Elbe estuary.

5 Conclusions

With the new estuarine model presented here, qualitatively satisfying results for the simulation of the forma-

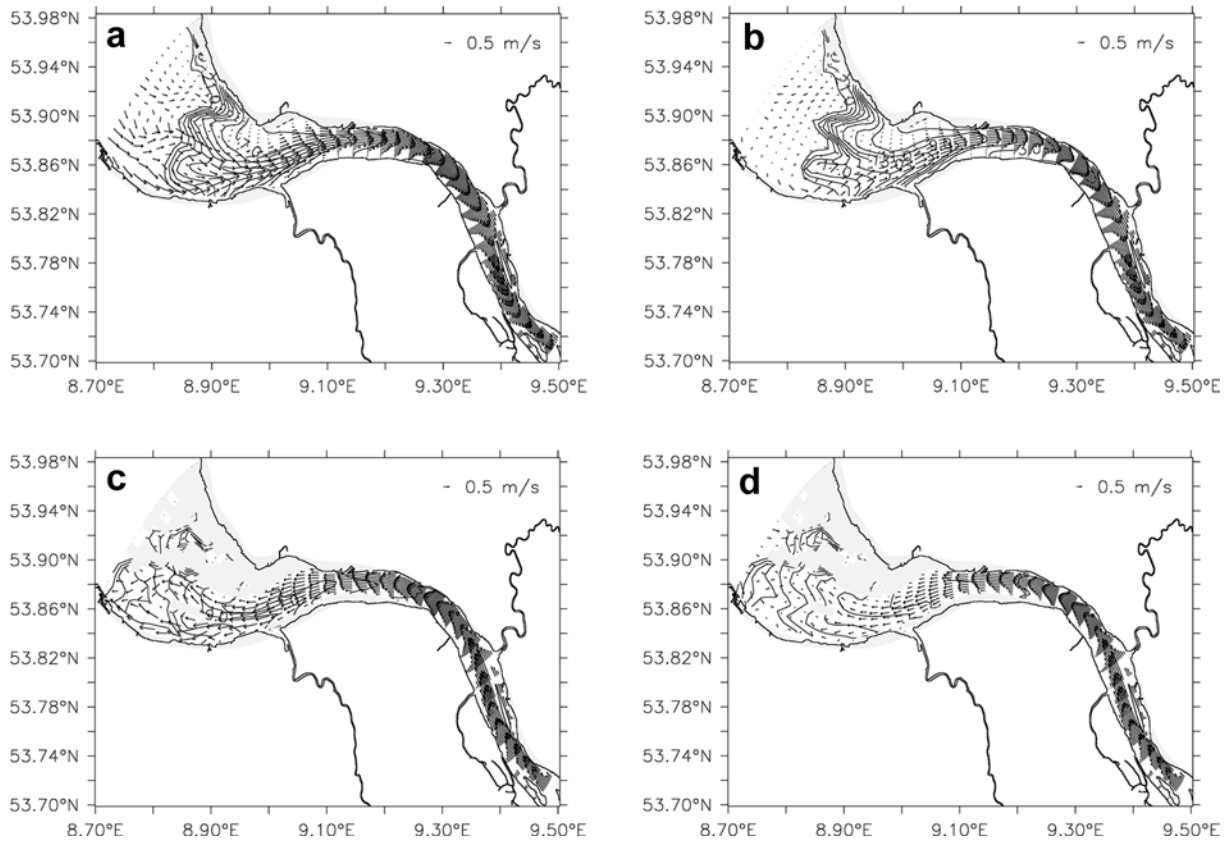

Fig. 9 Salinity (contours from 1 to 23 psu with intervals of 2 psu) and velocity in m s^{-1} for flood tide (*upper left*), slack flood tide (*upper right*), ebb tide (*lower left*) and slack ebb tide (*lower right*) at km 690. The maximum velocity is about 1.5 m s^{-1}. *Light grey shaded areas* correspond to cells that have fallen dry

tion of estuarine turbidity maxima (ETMs) could be achieved. With the idealised two-dimensional along-estuary experiment, the major ETM generation mechanisms (residual gravitational circulation and tidal mixing asymmetry) could be reproduced such that a pronounced ETM evolved from a spatially homogeneous SPM distribution in the region of the landward end of the salt wedge. In the three-dimensional simulation based on a realistic bathymetry of the Elbe estuary, an ETM developed after a couple of tidal periods. The location of this ETM was in agreement with observations for the typical river runoff and the mean tide chosen. Further weaker ETMs, usually also seen in the observations, have not been clearly reproduced, probably due to the fact that here only one size class (and thus one constant settling velocity) was used.

Since the transport equations for salt and suspended matter are based on mass conservation principles, the major requirement for the numerical schemes is mass conservation for these properties. This is properly fulfilled by the present model, mainly due to the consistent splitting of the external and the internal mode (see Burchard and Bolding 2002 for details). Also the presence of extensive tidal flats does not violate this conservation principle. To our knowledge, there is no other explicit baroclinic mode splitting model than the present model which allows for consistent (conservative) drying and flooding of intertidal flats. Since explicit mode-splitting models do resolve the barotropic mode with short time steps, it might be hypothesised that such models are advantageous for accurate drying and flooding processes compared to semi-implicit models using long time steps also for the barotropic mode. One other numerical challenge is the settling of suspended matter over these intertidal flats with minimum layer thicknesses of 10^{-3} m resulting from 20 vertical layers at a minimum depth of 0.02 m. With a settling velocity of 10^{-3} m s^{-1}, the CFL criterium for explicit advection schemes would dictate an internal time step of 1 s, much shorter than the model time step of about 37 s. The problem was solved by iterating the vertical advection in only these cells with a fractional time step as many times as necessary for fulfilling the CFL criterium (see Sect. 3.2).

The quantitative predictability of the model has not been tested with the model runs presented in this paper. For doing so, the simulation of hindcast scenarios with realistic boundary and meteorological forcing would be necessary, a complex challenge which is beyond the scope of the present study. Anyway, quantitative reproduction of observed SPM concentrations is extremely difficult due to lack of information concerning sediment composition, concentrations at the open boundaries and size class composition. Specifically, the

latter information is difficult to obtain due to the plethora of biogeochemical and small-scale physical processes which influence the size class composition on various time scales (see, e.g. van Leussen 1988 and Simenstad et al. 1995).

The underprediction of the tidal range increase towards Hamburg is a sign that the horizontal resolution of the model is not yet sufficient. The positive effect on accuracy of increasing the horizontal resolution for curvilinear grid has been shown for the present model by means of idealised channel flow (see Burchard and Bolding 2002, who also demonstrate the advantage of curvilinear grids over Cartesian grids for curved channels). The sensitivity of residual transports to the advection scheme for momentum has been demonstrated in the GETM report by Burchard and Bolding (2002): for a simulation of the Sylt-Rømø Bight the tidal residual transports were significantly increased when using a high-order TVD scheme rather than a first-order upstream scheme. The model sensitivity to vertical near-bed resolutions has been demonstrated by Burchard et al. (1999). They show that the choice of boundary condition discretisation for the turbulent quantitities is critical for the accurate reproduction of the logarithmic law. Potential improvements will be to apply higher order advection schemes also for turbulence advection. Advection of turbulent quantities is usually neglected in ocean models since the turbulent times scales are supposed to be significantly shorter than the advective time scales such that the effect is small (see Delhez et al. 1999). However, for estuaries where fronts are advected at high velocity, this practise probably needs to be revised. First tests with GETM show a significant effect of turbulence advection near fronts.

One other problem which always needs to be discussed with terrain-following coordinate models is not evident here: the truncation error of the internal pressure gradient approximation (see Haney 1991) which occurs for distinct stable stratification maxima (thermoclines, haloclines) when isopycnals are not parallel to coordinate surfaces. This problem is typically evident in situations where a stable stratification occurs over steep bathymetry. In such situations, the non-physical internal pressure gradient truncation error may be of the same order as other physical terms. In contrast to this, in macro-tidal estuaries with high energetics, the internal pressure gradient term is small compared to other terms such as the frictional force and the external (barotropic) pressure gradient. Thus, a general discussion of the pressure gradient error is beyond the scope of this paper. However, when applying the present model to micro-tidal estuaries such as fjords or the Baltic Sea, some discussion of this problem will be needed, see e.g. the recent comparative study carried out by Shchepetkin and Mc Williams (2003).

Acknowledgements The work of Karsten Bolding is partially funded by European projects MaBenE (EVKS-2001-00144) and OCEANIDES (EVK2-CT-3003-00277). The work of Manuel Ruiz Villarreal has been partially funded by a Marie Curie Fellowship of the European Community Programme IHP under contract number HPMF-CT-2000-01037. He also acknowledges the present support of a Ramón y Cajal fellowship (Spanish Ministery of Science and Technology). We wish to thank Marcus Böhlich (Bundesanstalt für Wasserbau Dienststelle Hamburg, Germany) for providing us with bathymetric data of the Elbe estuary. We are furthermore grateful to Jean-Marie Beckers (University of Liège, Belgium) for supporting the development of GETM with his ocean modelling expertise. We finally would like to thank two anonymous reviewers for their fruitful comments which helped to improve this manuscript.

References

Allen GP, Salomon JC, Bassoullet P, Du Penhoat Y, De Grandpre C (1980) Effects of tides on mixing and suspended sediment transport in macrotidal estuaries. Sedimentol Geol 26: 69–90

Backhaus JO (1985) A three-dimensional model for the simulation of shelf sea dynamics. Dt Hydrogr Z 38: 165–187

Beckers J-M (1991) Application of a 3D model to the Western Mediterranean. J Mar Sys 1: 315–332

Beckers J-M, Deleersnijder E (1993) Stability of a FBTCS scheme applied to the propagation of shallow-water inertia-gravity waves on various space grids. J Computat Phys 108: 95–104

Blumberg AF, Mellor GL (1987) A description of a coastal ocean circulation model. In: Heaps NS (ed) Three-dimensional ocean models. American Geophysical Union, Washington, DC pp. 1–16

Brenon I, LeHir P (1999) Modelling the turbidity maximum in the Seine estuary (France): identification of formation processes. Estuar Coast Shelf Sci 49: 525–544

Bryan K (1969) A numerical model for the study of the world ocean. J Computat Phys 4: 347–376

Burchard H (1995) Turbulenzmodellierung mit Anwendungen auf thermische Deckschichten im Meer und Strömungen in Wattengebieten. PhD Thesis, Institut für Meereskunde, Universität Hamburg, published as: Report 95/E/30, GKSS Research Centre

Burchard H (1998) Presentation of a new numerical model for turbulent flow in estuaries. In: Babovic V, Larsen LC (eds) Hydroinformatics '98 Balkema, Rotterdam, Proceedings of the 3rd International Conference on Hydroinformatics, Copenhagen, Denmark, 24–26 August 1998, pp 41–48

Burchard H (2002) Applied turbulence modelling in marine waters, vol 100. Lecture notes in Earth sciences. Springer, Berlin Heidelberg New York

Burchard H, Baumert H (1998) The formation of estuarine turbidity maxima due to density effects in the salt wedge. A hydrodynamic process study. J Phys Oceanogr 28: 309–321

Burchard H, Beckers J-M (2004) Non-uniform adaptive vertical grids in one-dimensional numerical ocean models. Ocean Model 6: 51–81

Burchard H, Bolding K (2001) Comparative analysis of four second-moment turbulence closure models for the oceanic mixed layer. J Phys Oceanogr 31: 1943–1968

Burchard H, Bolding K (2002) GETM – a general estuarine transport model. Scientific Documentation Tech Rep EUR 20253 EN European Commission

Burchard H, Petersen O (1997) Hybridisation between σ and z coordinates for improving the internal pressure gradient calculation in marine models with steep bottom slopes. Int J Numer Meth Fluids 25: 1003–1023

Burchard H, Petersen O (1999) Models of turbulence in the marine environment — a comparative study of two-equation turbulence models. J Mar Sys 21: 29–53

Burchard H, Bolding K, Villarreal MR (1999) GOTM – a general ocean turbulence model. Theory, applications and test cases. Tech Rep EUR 18745 EN European Commission

Cancino L, Neves R (1999) Hydrodynamic and sediment suspension modelling in estuarine systems, Part II. Application to the Western Scheldt and Gironde estuaries. J Mar Sys 22: 117–131

Canuto VM, Howard A, Cheng Y, Dubovikov MS (2001) Ocean turbulence. Part I: One-point closure model. Momentum and heat vertical diffusivities. J Phys Oceanogr 31: 1413–1426

Casulli V, Cattani E (1994) Stability, accuracy and efficiency of a semi-implicit method for three-dimensional shallow water flow. Computers Math Appl 27: 99–112

Casulli V, Cheng RT (1992) Semi-implicit finite difference methods for three-dimensional shallow water flow. Int J Numer Meth Fluids 15: 629–648

Cox MD (1984) A primitive equation, 3-dimensional model for the ocean. Tech Rep 1, Geophysical Fluid Dynamics Laboratory, University of Princeton, Princeton, NJ, 75 pp

de Kok JM (1992) A 3D finite-difference model for the computation of near- and far-field transport of suspend matter near a river mouth. Continental Shelf Res 12: 625–642

Deleersnijder E, Ruddick KG (1992) A generalized vertical coordinate for 3D marine problems. Bull Soc Roy Sci Liège 61: 489–502

Delhez EJM, Grégoire M, Nihoul JCJ, Beckers J-M (1999) Dissection of the GHER turbulence closure scheme. J Mar Sys 21: 379–397

Dippner J (1984) Ein Strömungs- und Öldriftmodell für die Deutsche Bucht Tech Rep Suppl 8, Veröff Inst Meeresforsch Bremerh

Duwe K (1988) Modellierung der Brackwasserdynamik eines Tideästuars am Beispiel der Unterelbe. PhD Thesis, Universität Hamburg In: Hydromod Publ. No. 1, Wedel, Hamburg

Duwe KC, Pfeiffer KD (1988) Three-dimensional modelling of transport processes in a tidal estuary and its implications for water quality management. In: Schreftler BA, Zienkiewicz OC (eds) Computer modelling in ocean engineering. Balkema, Brookfield, pp 419–426

Ezer T, Arango HG, Shchepetkin AF (2002) Developments in terrain-following ocean models: intercomparisons of numerical aspects. Ocean Model 4: 249–267

Festa JF, Hansen DV (1978) Turbidity maxima in partially mixed estuaries — a two-dimensional numerical model. Estuar Coast Mar Sci 7: 347–359

Flather RA, Heaps NS (1975) Tidal computations for Morecambe Bay. Geophys J Roy Astron Soc 42: 489–517

Freeman NG, Hale AM, Danard MB (1972) A modified sigma equations' approach to the numerical modeling of Great Lakes hydrodynamics. J Geophys Res 77: 1050–1060

Gerdes R (1993) A primitive equation ocean circulation model using a general vertical coordinate transformation, 1. Description and testing of the model. J Geophys Res 98: 14683–14701

Geyer WR, Farmer DM (1989) Tide-induced variation of the dynamics of a salt wedge estuary. J Phys Oceanogr 19: 1060–1072

Geyer WR, Signell RP, Kineke GC (1998) Lateral trapping of sediment in a partially mixed estuary. In: Dronkers J, Scheffers MBAM (eds) Physics of estuaries and coastal seas. Balkema, Rotterdam, Brookfield, pp 115–124

Haidvogel DB, Beckmann A (1999) Numerical ocean circulation modelling, vol. 2. Series on environmental science and management. Imperial College Press, London

Haidvogel DB, Arango HG, Hedstrom K, Beckmann A, Malanotte-Rizzoli P, Shchepetkin AF (2000) Model evaluation experiments in the North Atlantic basin: simulations in nonlinear terrain-following coordinates. Dyn Atmos Oceans 32: 239–281

Haney RL (1991) On the pressure gradient force over steep topography in sigma coordinate ocean models. J Phys Oceanogr 21: 610–619

Hundsdorfer W, Trompert RA (1994) Method of lines and direct discretisation: a comparison for linear adevction. Appl Numer Math 13: 469–490

Jay DA, Musiak JD (1994) Particle trapping in estuarine tidal flows. J Geophys Res 99: 445–461

Kantha LH, Clayson CA (2000) Numerical models of oceans and oceanic processes, vol. 66. International geophysics series. Academic Press, New York

Kappenberg J, Schymura G, Fanger HU (1995) Sediment dynamics and estuarine circulation in the turbidity maximum of the Elbe river. Neth J Aqu Ecol 29: 229–237

Kasahara A (1974) Various vertical coordinate systems used for numerical weather predictions. Monthly Weather Rev 102: 509–522

Krone RB (1962) Flume studies of the transport of sediment in estuarial shoaling processes. Tech. Rep. Hydraulic Engineering Laboratory, University of California, Berkeley, CA. 110 pp

Lang G, Schubert R, Markofsky M, Fanger H-U, Grabeman I, Kraseman L, Neumann L, Riethmüller R (1989) Data interpretation and numerical modeling of the mud and suspended sediment experiment 1985. J Geophys Res 94: 14381–14393

Launder BE, Reece GJ, Rodi W (1975) Progress in the development of a Reynolds-stress turbulence closure. J Fluid Mech 68: 537–566

Le Normant C, Peltier E, Teisson C (1998) Three-dimensional modelling of cohesive sediment transport in estuaries. In: Dronkers J, Scheffers MBAM (eds) Physics of estuaries and coastal seas. Balkema, Rotterdam, Brookfield, pp 65–71

Lobmeyr M, Puls W (1991) Modellrechnungen zum Schwebstofftransport: Vergleich der Ergebnisse eines zweidimensionalen Modells mit Feldmessungen im Elbästuar. Tech Rep GKSS 91/E/25, GKSS Research Centre, Geesthacht, Germany

Luyten PJ, Deleersnijder E, Ozer J, Ruddick KG (1996) Presentation of a family of turbulence closure models for stratified shallow water flows and preliminary application to the Rhine outflow region. Continental Shelf Res 16: 101–130

Madala RV, Piacsek SA (1977) A semi-implicit numerical model for baroclinic oceans. J Computat Phys 23: 167–178

Madec G, Delecluse P, Imbard M, Levy C (1998) OPA 8.1 Ocean General Circulation Model reference manual, Note du Pôle de modélisation, Institut Pierre–Simon Laplace, Paris, France, no. 11, 91 pp

Malcherek A (1995) Mathematische Modellierung von Strömungen und Stofftransportprozessen in Ästuaren. PhD Thesis, Institut für Strömungsmechanik und Elektron. Bericht Nr 44/1995, Rechnen im Bauwesen der Universität Hannover

Martins F, Leitão P, Silva A, Neves R (2001) 3D modeling in the Sado estuary using a new generic vertical discretization approach. Oceanologica Acta 24: S51–S62

Mellor GL, Yamada T (1982) Development of a turbulence closure model for geophysical fluid problems. Rev Geophys 20: 851–875

Nezu I, Nakagawa H (1993) Turbulence in open channel flows. Balkema, Rotterdam, Brookfield

Patankar SV (1980) Numerical heat transfer and fluid flow. McGraw-Hill, New York

Pedlosky J (1987) Geophysical fluid mechanics, 2nd ed. Springer, Berlin Heidelberg New York

Perels PAJ, Karelse M (1982) A two-dimensional, laterally averaged model for salt intrusion in estuaries. Tech Rep 262, Waterloopkundig Laboratorium. Delft Hydraulics Laboratory

Pfeiffer KD (1987) Ein dreidimensionales Wattmodell. Tech Rep GKSS 87/E/56, GKSS Research Centre, Geesthacht, Germany

Pietrzak J (1998) The use of TVD limiters for forward-in-time upstream-biased advection schemes in ocean modeling. Monthly Weather Rev 126: 812–830

Pietrzak J, Jacobson JB, Burchard H, Vested HJ, Petersen O (2002) A three-dimensional hydrostatic model for coastal and ocean modelling using a generalised topography following co-ordinate system. Ocean Model 4: 173–205

Postma H (1967) Sediment transport and sedimentation in the estuarine environment. In: Lauff GH (ed) Estuaries, Am Assoc Adv Sci Washington, DC, pp 158–179

Postma H, Kalle K (1955) Die Entstehung von Trübungszonen im Unterlauf der Flüsse, speziell im Hinblick auf die Verhältnisse in der Unterelbe. Dt Hydrogr Z 8: 138–144

Roe PL (1985) Some contributions to the modeling of discontinuous flows. Lect Notes Appl Math 22: 163–193

Rolinski S (1999) On the dynamics of suspended matter transport in the tidal river Elbe: description and results of a Lagrangian model. J Geophys Res 104: 26043–26057

Shchepetkin AF, McWilliams JC (2003) A method for computing horizontal pressure-gradient force in an oceanic model with a nonaligned vertical coordinate. J Geophys Res 108: 10.1029/2001JC001,047

Simenstad CA, Reed D, Jay DA, Prahl F, Small L, Baross JA (1995) LMER in the Columbia River Estuary: an interdisciplinary approach to investigating couplings between hydrological, geochemical and ecological processes. In: Dyer KR, Orth RJ (eds) Changing particle fluxes in estuaries: implications from science to management. Olsen and Olsen, Fredensborg pp. 437–444

Simpson JH, Brown J, Matthews J, Allen G (1990) Tidal straining, density currents, and stirring in the control of estuarine stratification. Estuaries 26: 1579–1590

Simpson JH, Burchard H, Fisher NR, Rippeth TP (2002) The semi-diurnal cycle of dissipation in a ROFI: model-measurement comparisons. Continental Shelf Res 22: 1615–1628

Song Y, Haidvogel DB (1994) A semi-implicit ocean circulation model using a generalised topography-following coordinate. J Computat Phys 115: 228–244

Stanev E, Wolff J-O, Burchard H, Bolding K, Flöser G (2003) On the circulation in the East Frisian wadden sea: numerical modelling and data analysis. Ocean Dynamics 53: 27–51

Stips A, Pohlmann T, Bolding K, Burchard H (2003) Simulating the temporal and spatial dynamics of the North Sea using the new model GETM (general estuarine transport model). Ocean Dynamics 54: 267–284

Strang G (1968) On the construction and comparison of difference schemes. SIAM J Num Anal 5: 506–517

Umlauf L, Burchard H (2003) A generic length-scale equation for geophysical turbulence models. J Mar Res 61: 235–265

Umlauf L, Burchard H, Hutter K (2003) Extending the k-ω turbulence model towards oceanic applications. Ocean Model 5: 195–218

van Leer B (1979) Toward the ultimate conservative difference scheme, V. A second-order sequel to Godunov's method. J Computat Phys 32: 101–136

van Leussen W (1988) Aggregation of particles, settling velocity of mud flocs: a review. In: Dronkers J, van Leussen W (eds) Physical processes in estuaries. Springer, Berlin Heidelberg, New York, pp 347–403

Villarreal MR, Montero P, Taboada J, Prego R, Leitão P, Villar VP (2001) Hydrodynamic model study of the Ria de Pontevedra under estuarine conditions. Estuar Coastal Shelf Sci 53: 101–113

Warner JC, Sherwood CR, Butman B, Arango HG, Signell RP (2003, Submitted) Implementation of a generic length scale turbulence closure into a 3D oceanographic model, Ocean Modelling

Wilcox DC (1998) Turbulence modeling for CFD, 2 ed., DCW Industries, La Cañada, California, 540 pp